Expanding the application of photoelectro-Fenton treatment to urban wastewater using the Fe(III)-EDDS complex

Zhihong Ye, Enric Brillas, Francesc Centellas, Pere Lluís Cabot, Ignasi Sirés*

Laboratori d'Electroquímica dels Materials i del Medi Ambient, Departament de Química Física,

Facultat de Química, Universitat de Barcelona, Martí i Franquès 1-11, 08028 Barcelona, Spain

* Corresponding author: i.sires@ub.edu (I. Sirés)

1

Abstract

This work reports the first investigation on the use of EDDS as chelating agent in photoelectro-Fenton (PEF) treatment of water at near-neutral pH. As a case study, the removal of the antidepressant fluoxetine was optimized, using an electrochemical cell composed of an IrO_2-based anode an air-diffusion cathode for in-situ H_2O_2 production. Electrolytic trials at constant current were made in ultrapure water with different electrolytes, as well as in urban wastewater (secondary effluent) at pH 7.2. PEF with Fe(III)–EDDS (1:1) complex as catalyst outperformed electro-Fenton and PEF processes with uncomplexed Fe(II) or Fe(III). This can be explained by: (i) the larger solubilization of iron ions during the trials, favoring the production of $^\bullet OH$ from Fenton-like reactions between H_2O_2 and Fe(II)–EDDS or Fe(III)–EDDS, and (ii) the occurrence of Fe(II) regeneration from Fe(III)–EDDS photoreduction, which was more efficient than conventional photo-Fenton reaction with uncomplexed Fe(III). The greatest drug concentration decays were achieved at low pH, using only 0.10 mM Fe(III)–EDDS in a 1:1 molar ratio, although complete removal in wastewater was feasible only with 0.20 mM Fe(III)–EDDS due to the greater formation of $^\bullet OH$. The effect of the applied current and anode nature was rather insignificant. A progressive destruction of the catalytic complex was unveiled, whereupon the mineralization mainly progressed thanks to the action of $^\bullet OH$ adsorbed on the anode surface. Despite the incomplete mineralization using BDD as the anode, a remarkable toxicity decrease was determined. Fluoxetine degradation yielded F^- and NO_3^- ions, along with several aromatic intermediates. These included two chloro-organics, as a result of the anodic oxidation of Cl^- to active chlorine. A detailed mechanism for the Fe(III)–EDDS-catalyzed PEF treatment of fluoxetine in urban wastewater is finally proposed.

Keywords: Ethylenediamine-*N,N'*-disuccinic (EDDS) acid; Fluoxetine; Gas-diffusion electrode; Hydrogen peroxide; Photoelectro-Fenton; Urban wastewater

1. Introduction

Fenton's reaction (reaction (S1) in Table S1) has promoted the development of one of the most successful subtypes within the advanced oxidation processes (AOPs) for the degradation of organic pollutants in water (Brillas et al., 2009; Zhou et al., 2018). Indeed, Fenton process allows their fast removal thanks to the production of •OH in the bulk solution, showing great potential to be integrated as a tertiary treatment in urban wastewater treatment facilities (WWTFs) (Zhang et al., 2019). Nevertheless, the risk, environmental impact and cost related to H_2O_2 synthesis, storage, transportation and handling is a major handicap. Fortunately, electrolyzers for in-situ H_2O_2 production from the two-electron reduction of gaseous O_2 (reaction (1)) have been devised in recent years (Brillas et al., 2009) and, among them, those equipped with a carbon-based air-diffusion cathode yield the largest accumulation of this oxidant upon facile modulation of input current (Sirés et al., 2007; Galia et al., 2016; Roth et al., 2016; Lanzalaco et al., 2017; Coria et al., 2018; Pérez et al., 2018).

$$O_2(g) \ + \ 2 \ H^+ \ + \ 2 \ e^- \ \rightarrow \ H_2O_2 \tag{1}$$

In the most simple configuration of electrochemical AOPs, a cathode with ability to electrogenerate H_2O_2 is combined with boron-doped diamond (BDD) (Panizza and Cerisola, 2009; Martínez-Huitle et al., 2015; Clematis et al., 2017) or a dimensionally stable anode (DSA®) based on IrO_2 (Scialdone et al., 2009; Lanzalaco et al., 2017, 2018) or RuO_2 (Ribeiro and De Andrade, 2004; Xu et al., 2017). Such high oxidation power anode materials (M) allow the production of adsorbed M(•OH) via water oxidation, giving rise to the electro-oxidation (EO) process. If iron catalyst is present in the contaminated solution, the process is so-called electro-Fenton (EF). The Fe(II) regeneration is feasible from Fe(III) reduction when a large surface area cathode like carbon felt is employed (El-Ghenymy et al., 2014; Yahya et al., 2014; Yang et al., 2019). A more effective Fe(II) regeneration route, compatible with all kinds of cathode materials, arises from Fe(III) photoreduction. Classical photo-Fenton reaction (2) at optimum pH ~ 2.8 involves the continuous

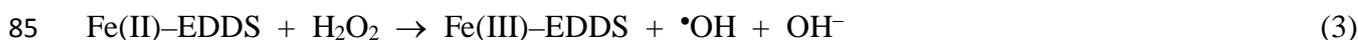57   reduction of hydrated Fe^{3+} ion with concomitant $^\bullet OH$ production, thanks to ligand-to-metal charge

58   transfer (LMCT) occurring under UVA irradiation. Accordingly, photoelectro-Fenton (PEF)

59   process has experienced an intense development with outstanding results (Flores et al., 2016; Steter

60   et al., 2016; Komtchou et al., 2017; Alcocer et al., 2018; Aveiro et al., 2018; Vidal et al., 2018;

61   Wang et al., 2018; Oriol et al., 2019).

62    $$[Fe(OH)]^{2+} + h\nu \rightarrow Fe^{2+} + {}^\bullet OH \qquad\qquad (2)$$

63   EF and PEF have been proven very successful at acidic pH, which is mainly due to total

64   solubilization of iron ions. Conversely, higher pH results in a considerable efficiency loss because

65   of iron precipitation. For some time this has been an obstacle, impeding the application to urban

66   wastewater treatment, but two smart solutions are currently available: (i) heterogeneous Fenton

67   processes, employing iron catalyst in solid form (Zhou et al., 2018), and (ii) modified homogeneous

68   Fenton processes, employing chelated iron as a soluble species (Clarizia et al., 2017). A priori, the

69   latter option seems more appealing because it is expected to yield faster removals.

70   Only some few recent articles have assessed the performance of EF and PEF in urban

71   wastewater, although chelated iron has never been used (Komtchou et al., 2015; Ridruejo et al.,

72   2018; Guelfi et al., 2019a; Villanueva-Rodríguez et al., 2019; Ye et al., 2019a). Note that, in this

73   kind of complex water matrix, the oxidation of Cl^- anion at the anode surface yields additional

74   oxidants like active chlorine (Cl_2 and ClO^-) along with chlorine radicals (Table S1) (Panizza and

75   Cerisola, 2009). Carboxylates like oxalate and citrate have been two widely used chelating agents in

76   non-electrochemical Fenton treatments (Ye et al., 2019c). However, polydentate ligands like

77   nitrilotriacetic (NTA), ethylenediaminetetraacetic (EDTA) and ethylenediamine-N,N'-disuccinic

78   (EDDS) acids seem more interesting to ensure iron complexation (Clarizia et al. 2017).

79   Furthermore, they enhance the LMCT because of their typically higher molar absorption

80   coefficients in the near-UV and visible regions. Among polydentate ligands, EDDS is advantageous

81   for photo-Fenton process. It forms soluble Fe(II)–EDDS and Fe(III)–EDDS complexes at a wide pH

4

range, favoring the occurrence of reactions (3) and (4) at near-neutral pH that mimic Fenton's

reaction (S1) and Fenton-like reaction (S2) (Zhang et al., 2016). Note that superoxide radical ($O_2^{\bullet-}$)

originated in the latter reaction is transformed into $HO_2^{\bullet}$ at pH > 4.8-4.9 (reaction S9).

$$\text{Fe(II)–EDDS} + H_2O_2 \rightarrow \text{Fe(III)–EDDS} + {}^{\bullet}\text{OH} + \text{OH}^- \tag{3}$$

$$\text{Fe(III)–EDDS} + H_2O_2 \rightarrow \text{Fe(II)–EDDS} + O_2^{\bullet-} + 2H^+ \tag{4}$$

In spite of being a structural isomer of the persistent pollutant EDTA (Yuan and VanBriesen 2006), it is considered a biodegradable substance. Mailhot and co-workers introduced for the first time EDDS in Fenton and photo-Fenton processes (Huang et al., 2012, 2013; Li et al., 2010; Wu et al., 2014). Since then, only some few works have explored the degradation of organic micropollutants by Fe(III)–EDDS-assisted photo-Fenton (Papoutsakis et al., 2015) and solar photo-Fenton (Soriano-Molina et al., 2018, 2019; Cuervo Lumbaque et al., 2019). It has been demonstrated that photo-Fenton-like reaction (5) exhibits a much higher quantum yield than conventional photo-Fenton reaction (2): 0.017 for the latter at 360 nm (Safarzadeh-Amiri et al., 1997) versus 0.10 for the former at 290-400 nm (Wu et al., 2014). In addition, the Fe(III)–EDDS complex is able to absorb in the visible region.

$$\text{Fe(III)–EDDS} + h\nu \rightarrow \text{Fe}^{2+} + \text{EDDS}^{\bullet+} \tag{5}$$

Based on these positive features, it is expected that Fe(III)–EDDS complex is also advantageous in PEF process. We have recently elucidated the mechanism of EF treatment with Fe(III)–EDDS (Ye et al., 2019b), but there is no article that discusses its particularities in PEF and the further application to the removal of pharmaceuticals in urban wastewater matrices. The occurrence of pharmaceutical residues and their transformation products in water, which mainly results from the absence or inefficiency of treatments at WWTFs (Bagnis et al., 2018; Kümmerer et al., 2019), has become a big obstacle to global water quality, posing serious threats to humans and ecosystems. Prozac® is one of the top-selling antidepressants worldwide, being the fluorinated molecule fluoxetine its active ingredient. This pollutant has been detected in effluents from WWTFs

in the Baltic Sea (UNESCO, 2017). In Canada and China, fluoxetine has been detected in effluents from WWTFs and freshwater at ng L^{-1} level (Jennifer Ebele et al., 2017), being also detected in marine environment (Mezzelani et al., 2018). Fluoxetine has a proven ecotoxicological impact at environmental level (Desbiolles et al., 2018) and, as a result, it has been included in some list of priority substances (Jennifer Ebele et al., 2017). Several electrochemical technologies have been developed in recent years to enhance the removal of pharmaceuticals from water (Brillas and Sirés, 2015). In particular, fluoxetine was treated by EO with TiO_2 and PbO_2 (Wang et al., 2018). The great performance of EF and PEF has also been ascertained, using a BDD/air-diffusion cell, but only in a model aqueous matrix with 0.050 M Na_2SO_4 at pH 3.0 (Salazar et al., 2017).

To our knowledge, this is the first study dedicated to the Fe(III)–EDDS-catalyzed PEF process, which has been applied to the treatment of the pharmaceutical fluoxetine at circumneutral pH. The degradation performance was evaluated from high-performance liquid chromatography (HPLC) and total organic carbon (TOC) data. Most of the electrolyses have been carried out using an IrO_2/air-diffusion cell at constant current, both in urban wastewater and in model matrices to better assess the effect of key parameters like catalyst source, Fe(III)–EDDS dosage, Fe(III):EDDS ratio, pH or applied current on the concentrations of Fe(II) and Fe(III), Fe(III)–EDDS complex and H_2O_2. The main reaction by-products were identified by gas chromatography-mass spectrometry (GC-MS) and ion chromatography, whereas toxicity was assessed from Microtox® analysis.

2. Experimental

2.1. Chemicals

Fluoxetine hydrochloride (certified reference material) was purchased from Sigma-Aldrich. Sodium sulfate, heptahydrated iron(II) sulfate, sulfuric acid (96-98% solution) and sodium hydroxide pellets were of analytical grade from Merck, Panreac and J.T. Baker. $Fe(ClO_4)_3$ and EDDS trisodium salt solution (~ 35% aqueous solution) used to prepare the catalytic complex were

131   purchased from Sigma-Aldrich. $TiOSO_4$ and 1,10-phenanthroline monohydrate employed for H_2O_2

132   and dissolved iron quantification, respectively, were from Sigma-Aldrich and Alfa Aesar. All the

133   other chemicals were of analytical or HPLC grade supplied by Merck and Panreac.

134   *2.2. Aqueous matrices employed to dissolve fluoxetine hydrochloride*

135   The electrolytic trials were made with 150 mL of two different kinds of solutions:

136   (i) 0.050 M Na_2SO_4 in Millipore Milli-Q water (resistivity > 18 MΩ cm at 25 ℃), whose

137   natural pH was around 5.7;

138   (ii) wastewater collected from the secondary effluent of a WWTF placed near Barcelona, at

139   natural pH 7.2. Before use, the wastewater was preserved in a refrigerator at 4 ℃, which allowed

140   making all the experiments with water from the same batch. This urban wastewater had a specific

141   conductivity of 1.35 mS cm^{-1}, total carbon content of 119.5 mg L^{-1} and TOC of 9.3 mg L^{-1}. The

142   concentration of cations was: 0.11 mg L^{-1} Fe^{2+}, 33.9 mg L^{-1} Mg^{2+}, 94.0 mg L^{-1} Ca^{2+}, 46.8 mg L^{-1} K^+

143   and 315.9 mg L^{-1} Na^+. The content of anions was: 4.2 mg L^{-1} NO_2^-, 16.9 mg L^{-1} NO_3^-, 569.8 mg L^{-1}

144   Cl^- and 128.4 mg L^{-1} SO_4^{2-}. In most of the experiments, the wastewater was first conditioned: it

145   was acidified to pH around 2.0 using H_2SO_4 solution; then, the volatile compounds where stripped

146   under nitrogen stream, and pH was re-established with NaOH solution. Table S2 summarizes the

147   seven organic compounds clearly identified in this aqueous sample.

148   When required, fluoxetine hydrochloride was spiked into the aqueous matrices at 0.049 mM

149   (i.e., 10 mg L^{-1} TOC). For the preparation of the Fe(III)–EDDS (1:1) complex, 10 mM $Fe(ClO_4)_3$

150   and 10 mM EDDS solutions were prepared and stored in amber glass bottles. For each experiment,

151   a fresh complex was prepared by mixing equal volumes in the dark. The mixture was stirred for 3

152   min, thereby withdrawing a small volume that was added to the fluoxetine solution. A similar

153   procedure was followed to prepare complexes with other Fe(III):EDDS ratios. In some cases,

154    $FeSO_4$ and $Fe(ClO_4)_3$ were used as uncomplexed catalysts for comparison.

2.3. Electrochemical systems

All the experiments were made in an undivided, jacketed glass cell. The cell contained 150 mL of contaminated solution, thermostated at 25 ℃ and stirred with a magnetic PTFE follower at 700 rpm, and a pair of electrodes (each of them with 3 cm^2 immersed geometric area) separated 1 cm from each other. A sketch of a similar setup can be seen elsewhere (Oriol et al., 2019). The air-diffusion cathode, made of carbon-PTFE on carbon cloth (Sainergy Fuel Cell), was continuously fed with air at 1 L min^{-1} to ensure the H_2O_2 electrogeneration. Three different anodes were employed in this study: Ti|IrO$_2$-based and Ti|RuO$_2$-based plates purchased from NMT Electrodes, and a Si|BDD plate from NeoCoat. Constant current was applied between the anode and cathode by means of an Amel 2049 potentiostat-galvanostat, whereas the voltage between both electrodes was continuously monitored on a Demestres 601BR digital multimeter. Prior to first use, all the electrodes were activated upon electrolysis in a 0.050 M Na$_2$SO$_4$ solution at 300 mA for 180 min. In all trials, except in UVA photolysis and EO, iron sources were added as catalyst. In UVA photolysis and PEF, the solution was irradiated with UVA light (λ_{max} = 360 nm, irradiance of 5 W m^{-2} as measured with a Kipp&Zonen CUV 5 UV radiometer) provided by a 6-W Philips TL/6W/08 black light blue fluorescent tube placed at 7 cm above the liquid surface.

2.4. Analytical methods

The electrical conductance of the raw wastewater was determined with a Metrohm 644 conductometer. The pH of all solutions, before and after the trials, was measured with a Crison GLP 22 pH-meter. All subsequent analyses were carried out after filtration of the samples with PTFE filters (0.45 μm) from Whatman. The concentration of H_2O_2 accumulated during the electrochemical assays was determined spectrophotometrically, since it formed a yellow complex with a Ti(IV) reagent that presented a maximum absorbance at λ = 408 nm (Welcher, 1975). A Unicam UV/Vis device thermostated at 25 ℃ was employed for these analyses, as well as for dissolved iron quantification. The total dissolved Fe(II) concentration was determined at λ = 510

nm upon direct reaction with 1,10-phenanthroline, whereas Fe(III) was determined in the same manner after mixing with ascorbic acid since this allows quantifying the total dissolved iron content upon complete conversion of Fe(III) into Fe(II). The TOC content of the samples was immediately measured after collection, using a Shimadzu TOC-VCSN analyzer that yielded values with $\pm1\%$ accuracy. A Shimadzu TNM-1 unit coupled to the previous analyzer allowed the determination of total nitrogen (TN).

The decay of fluoxetine concentration was assessed by reversed-phase HPLC after preserving the withdrawn samples by dilution with acetonitrile. This analysis was made by injecting the diluted samples into a Waters 600 liquid chromatograph equipped with a BDS Hypersil C18 5μm (250 mm × 4.6 mm) column at 25 °C and coupled to a Waters 996 photodiode array detector selected at λ = 227 nm. A 50:50 (v/v) CH_3CN/H_2O (0.010 M KH_2PO_4) mixture at pH 3.0 was eluted at 1.0 mL min^{-1} as mobile phase, allowing the detection of fluoxetine at retention time t_r = 13.2 min. The concentration of the Fe(III)–EDDS complex was determined with the same equipment but using a solution with 2 mM tetrabutylammonium hydrogensulfate and 15 mM sodium formate as the aqueous phase at pH 4.0, which was mixed with methanol (95:5, v/v) and eluted at 0.8 mL min^{-1} as mobile phase. The detector was set at 240 nm and the complex appeared at t_r = 10.7 min. All trials for HPLC analysis were made twice, and samples were injected at least in duplicate. Average values with the corresponding error bars are reported in the figures.

The concentration of accumulated inorganic ions was obtained by ion chromatography using a Shimadzu 10Avp liquid chromatograph fitted with a Shim-Pack IC-A1S (100 mm × 4.6 mm) anion column at 40 °C, coupled to a Shimadzu CDD 10Avp conductivity detector. Measurements were conducted with a solution composed of 2.4 mM tris(hydroxymethyl)aminomethane and 2.6 mM phthalic acid, at pH 4.0, eluted at 1.5 mL min^{-1} as mobile phase. Peaks appeared at t_r of 1.75 min (F^-), 2.5 min (Cl^-) and 4.0 min (NO_3^-). The NH_4^+ concentration was obtained as reported elsewhere (Guelfi et al., 2019b).

The concentration of metal cations in the real wastewater and total dissolved iron during the trials was analysed by inductively coupled plasma optical emission spectroscopy (ICP-OES) using an Optima 3200L spectrometer from Perkin Elmer.

To assess the toxicity of untreated and treated solutions, acute bioluminescence inhibition assays were performed using the marine bacteria *Vibrio fischeri*. First, all the collected samples were treated to adjust their pH to 7.0, being subsequently diluted. The acute ecotoxicity was measured after 15 min of incubation at 25 °C using an AFNOR T90-301 Microtox® system. The bioluminescent bacteria and other reagents were supplied by Modern Water and the analysis was conducted following the standard procedure recommended by the manufacturer. Results obtained are expressed as EC_{50} (in $mg\,L^{-1}$), which accounts for the concentration of solution at a given electrolysis time that causes the reduction of the 50% of bioluminescence intensity upon contact with the bacteria for 15 min.

Organic compounds contained in the real wastewater, as well as stable organic by-products accumulated during the electrochemical treatment of fluoxetine either in 0.050 M Na_2SO_4 or conditioned wastewater were identified by GC-MS, comparing with NIST05 database. The organic components were extracted with 75 mL of CH_2Cl_2 in three times, followed by thorough drying over anhydrous Na_2SO_4, filtration and concentration under reduced pressure. The analysis was carried out on a 6890N gas chromatograph coupled to a 5975C mass spectrometer, both from Agilent Technologies, in EI mode at 70 eV. Non-polar Teknokroma Sapiens-X5ms and polar HP INNOWax columns (0.25 µm, 30 m × 0.25 mm) were employed. The temperature was increased from 36 ºC (1 min), up to 320 ºC (hold time of 10 min) for the former and 250 ºC for the latter, at 5 ºC min^{-1}, with the inlet and source at 250 and 230 ºC. The transfer line was at 280 ºC or 250 ºC, respectively.

## 3. Results and discussion

3.1. Fluoxetine degradation in 0.050 M Na$_2$SO$_4$ solutions at near-neutral pH

3.1.1. Comparative fluoxetine degradation by different methods

Since the main goal of this work was to employ the Fe(III)–EDDS complex as a photoactive catalyst in PEF process assisted with UVA light, its stability was first assessed in 0.050 M Na$_2$SO$_4$ medium at natural pH ~ 5.7, both in the dark and under UVA irradiation (Fig. S1). The 1:1 ratio was selected because it is presumed as the most photoactive (Wu et al., 2014). Fig. S1a highlights the high stability of the catalytic complex for 60 min in the dark at near-neutral pH. Conversely, in Fig. S1b, the great photoactivity of the Fe(III)–EDDS complex is evidenced, thus confirming the occurrence of photo-Fenton-like reaction (5).

In Fig. 1, the degradation of 0.049 mM fluoxetine in 0.050 M Na$_2$SO$_4$ medium at natural pH ~ 5.7 upon the application of different treatments is compared. Fig. 1a shows the null effect of UVA radiation alone, as expected from the absence of absorption of fluoxetine at such wavelength. In contrast, a substantial decay of 34% at 60 min was achieved in an analogous trial made in the presence of 0.1 M Fe(III)–EDDS (1:1) complex. The absence of cathodic H$_2$O$_2$ production could presumably discard the contribution of Fenton-based reactions (see Fig. S2 for a more detailed explanation). Therefore, the destruction of fluoxetine can be explained by the oxidative action of two types of radicals: (i) EDDS$^{\bullet+}$, which is formed along with Fe^{2+} via reaction (5), and pre-eminently (ii) O$_2^{\bullet-}$, whose presence has been confirmed from reaction (6) in aerated solutions at near-neutral pH (Hayyan et al., 2016).

$$Fe^{2+} + O_2 \rightarrow Fe^{3+} + O_2^{\bullet-} \tag{6}$$
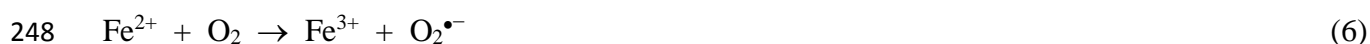
All the other trials included in Fig. 1 were carried out using the IrO$_2$/air-diffusion cell at 50 mA. In the absence of catalyst (EO process), a poor drug disappearance of 24% was attained, as a result of the low oxidation power of IrO$_2$($^{\bullet}$OH) radicals and their confinement in the electrode vicinity. Moreover, IrO$_2$($^{\bullet}$OH) was consumed to a large extent in the oxidation of H$_2$O$_2$, whose concentration was high and greater than that from fluoxetine because of the use of the efficient air-

254 diffusion cathode (see below). In contrast, a very small addition of Fe(III)–EDDS complex to the

255 initial solution caused a great enhancement of fluoxetine concentration decay, reaching 69% at 60

256 min. This was due to the production of a large amount of $O_2^{\bullet-}$ from reaction (4), which is in

257 equilibrium with its protonated form, $HO_2^{\bullet}$. In this EF process, the catalytic complex mainly existed

258 as Fe(III)–EDDS, because the air-diffusion cathode has low ability for its electroreduction (Ye et

259 al., 2019b). However, Fe(II)–EDDS formed as product in reaction (4) was able to react with H_2O_2

260 and generate $^{\bullet}OH$ via reaction (3). The final drug concentration decay in EF process when the

261 chelated complex was replaced by $FeSO_4$ was also partial, although slightly higher (72%) and with

262 a steeper profile, especially in the first minutes. Four factors could contribute to this behavior: (i)

263 the presence of hydrated Fe^{2+} ions from the beginning promoted the production of $^{\bullet}OH$ from

264 Fenton's reaction (S1); (ii) the oxidation of Fe^{2+} to Fe^{3+} from reaction (6) yielded $O_2^{\bullet-}$; (iii) the low

265 solubility of Fe^{2+} and Fe^{3+} at near-neutral pH caused the precipitation of most of the iron as

266 $Fe(OH)_3$, which could favor the fluoxetine disappearance by coagulation and heterogeneous

267 Fenton's reaction (see subsection 3.2); and (iv) the absence of a competing target like EDDS

268 allowed the action of all radicals and coagulants simply on fluoxetine (and its intermediates).

269 Fig. 1b reveals the greater performance of all PEF treatments. Up to 88% fluoxetine was

270 removed at 60 min using $FeSO_4$ in the absence of EDDS, although the profile during the first 10

271 min was very similar to that obtained in EF with the same catalyst (Fig. 1a). This means that in that

272 stage, the predominant degradation mechanism was the oxidation with the very oxidizing $^{\bullet}OH$

273 formed from conventional Fenton's reaction. After 10 min, UVA light in PEF allowed the

274 continuous regeneration of Fe^{2+} from dissolved Fe^{3+} according to photo-Fenton reaction (2).

275 Coagulation and heterogeneous Fenton's reaction with $Fe(OH)_3$ and oxidation by less powerful

276 radicals mentioned above could also contribute to gradual drug disappearance. A similar fluoxetine

277 concentration decay (83%) but with much lower conversion rate was observed using $Fe(ClO_4)_3$ as

278 catalyst. This agrees with the previous treatment, since the mechanism was exactly the same but the

279   absence of hydrated Fe^{2+} from the beginning impeded a faster initial fluoxetine disappearance.

280   Finally, PEF with 0.1 mM Fe(III)–EDDS (1:1) complex was clearly superior to all the other

281   treatments, being the only one that led to total drug abatement at 60 min. The used of chelated

282   Fe(III) was advantageous because: (i) it kept a higher amount of dissolved iron for longer time, in

283   contrast to EF and PEF without EDDS, and (ii) the UVA radiation allowed that the main form of

284   such dissolved iron was Fe(II)–EDDS, in contrast to all the EF systems. This resulted in the largest

285   production of $^{\bullet}OH$ via reaction (3), which degraded most of the fluoxetine molecules prior to

286   significant degradation of EDDS (see Fig. S2). The contribution of additional routes like

287   coagulation, heterogeneous Fenton's reaction and oxidation with other radicals cannot be discarded

288   either, since they could justify that the degradation was almost as fast as that previously achieved

289   for 0.049 mM fluoxetine with 0.050 M Na_2SO_4 at pH 3.0 by PEF using a BDD/air-diffusion cell at

290   a much higher current (300 mA) (Salazar et al., 2017). The inset panel in Fig. 1b shows the pseudo-

291   first-order kinetics in PEF with Fe(III)–EDDS, yielding an apparent rate constant $k_1 = 0.0986$ min^{-1}

292   ($R^2 = 0.987$).

293   *3.1.2. Evolution of iron ions, dissolved iron and generated H_2O_2*

294   In order to better explain the trends of most of the aforementioned treatments, the evolution of

295   concentrations of Fe(II), Fe(III), dissolved iron and H_2O_2 is depicted in Fig. S2a-c, whereas the

296   normalized Fe(III)–EDDS concentration can be seen in Fig. S2d. In UVA photolysis with 0.10 mM

297   Fe(III)–EDDS, the almost complete photoreduction of chelated Fe(III) to Fe^{2+} can be deduced from

298   Fig. S2a,b, thus confirming the occurrence of photo-Fenton-like reaction (5) as discussed in Fig. 1a.

299   In 30 min, 91% of Fe(III) was transformed into Fe^{2+}. The rest was soluble Fe(III), rather in

300   uncomplexed form because Fig. S2d highlights the total disappearance of the Fe(III)–EDDS

301   complex at 60 min. Worth noting, Fig. S2c shows the accumulation of a low amount of H_2O_2 in this

302   process. This phenomenon can be explained by reaction (S5), promoted by $O_2^{\bullet-}$, and suggests that

303   fluoxetine decay in UVA photolysis (Fig. 1a) was also due to the action of $^{\bullet}OH$ formed from

13

Fenton's reaction. Since EDDS$^{\bullet+}$ was also generated from reaction (5), the H$_2$O$_2$ accumulation could also be largely attributed to reaction (7) (Wu et al., 2014).

$$EDDS^{\bullet+} + O_2 \rightarrow EDDS_{OX} + H_2O_2 \tag{7}$$

In Fe(III)–EDDS-catalyzed EF, Fig. S2a,b confirm that the prevailing iron form was Fe(III), with only a minor production of Fe(II). In fact, from Fig. S2d, it is clear that such ion mainly existed as Fe(III)–EDDS. Furthermore, the iron precipitation was particularly evident from 30 min, losing 42% of dissolved iron at the end of the treatment. The presence of only a very low amount of $^\bullet$OH, formed as explained above, preserved the integrity of the Fe(III)–EDDS, but turned out to be detrimental for fluoxetine degradation (Fig. 1a). In PEF with Fe(ClO$_4$)$_3$ as catalyst, the most relevant feature was the very low dissolved iron concentration at time zero (i.e., 1.5 mg L^{-1}), which matched almost perfectly with Fe(III) concentration and decayed even more along the electrolysis. This suggests that fluoxetine concentration decay described for this process in Fig. 1b could be mainly due to coagulation with solid Fe(OH)$_3$. The H$_2$O$_2$ trends in Fig. S2c support this idea, because the profiles for EF with Fe(III)–EDDS, PEF with Fe(ClO$_4$)$_3$ and EO were almost coincident, which means that the reactions between H$_2$O$_2$ and complexed Fe(III)–EDDS (i.e., Fenton-like reaction) or precipitated Fe(OH)$_3$ (i.e., heterogeneous Fenton's reaction) were not so relevant. Finally, the aforementioned superiority of Fe(III)–EDDS-catalyzed PEF can be understood from Fig. S2a-d. This treatment allowed the accumulation of up to 1.7 mg L^{-1} Fe(II) (i.e., ~30% Fe(III) photoreduction from reaction (5), Fig. S2a) in 20 min, whereupon this content decayed progressively because of the gradual iron precipitation (Fig. S2b) and the almost total disappearance of the very photoactive Fe(III)–EDDS complex (Fig. S2d). Hence, in the absence of enough EDDS, coagulation with Fe(OH)$_3$ probably contributed to fluoxetine disappearance (Fig. 1b). Note that as a result of the greater presence of Fe(II) in this treatment, which stimulated Fenton's reaction, the accumulated H$_2$O$_2$ concentration was lower than in the previous processes (3.5 mM vs $\geq$ 5.0 mM, Fig. S2c). It is interesting to observe that fluoxetine (and its reaction intermediates) played a

14

protective role that enhanced the catalytic power of PEF process, as deduced when the latter

treatment was carried out in the absence of the drug. In that trial, the Fe(III)–EDDS complex

disappeared much more quickly (Fig. S2d), because the $^{\bullet}OH$ formed once the Fe^{2+} was

photoregenerated mainly participated in the destruction of EDDS. This led to a much faster iron

precipitation (Fig. S2b), with a consequently poor Fe(II) regeneration (Fig. S2a).

Aiming to clarify the role of oxidizing radicals during the fast degradation of fluoxetine by the

Fe(III)–EDDS-catalyzed PEF treatment, the experiment discussed in Fig. 1b was performed in the

presence of a radical scavenger. As can be seen in Fig. S3, the use of *p*-benzoquinone as a well-

known $O_2^{\bullet-}$ scavenger ($k_2 \sim 1 \times 10^9$ M^{-1} s^{-1}) caused a slow and evident deceleration of the drug

degradation, only attaining 88% degradation at 60 min. This trend suggests the participation of $O_2^{\bullet-}$

as oxidant in this PEF process, being mainly produced upon Fe(III)–EDDS photolysis with UVA

light as explained in Fig. 1a. However, Fig. S3 allows confirming that the prevalent radical was

$^{\bullet}OH$ because an analogous trial in the presence of *tert*-butanol as single scavenger ($k_2 = 6.8 \times 10^9$ M^{-1}

s^{-1}) revealed the very slow fluoxetine concentration decay, with a disappearance of 17% as maximal

at the end of the electrolysis.

3.1.3. Detection of inorganic ions and effect of experimental variables during PEF treatment

In order to have a first idea about the changes undergone by the fluoxetine structure during the

PEF treatment with chelated iron, the inorganic ions accumulated in solution were analyzed. A

higher drug concentration as compared to all previous trials, i.e., 0.098 mM, was employed to allow

a more accurate quantification. Considering that the pollutant was in the form of hydrochloride, this

corresponded to a content of 1.4 mg L^{-1} N, 3.5 mg L^{-1} Cl and 5.6 mg L^{-1} F. Fig. S4 confirms the

presence of 3.4 mg L^{-1} Cl^- in the initial solution, but this concentration decreased gradually along

the electrolysis. At 60 min, 12% of Cl^- ion was converted to active chlorine (Cl_2 + ClO^-), with no

traces of chlorine oxyanions (ClO_2^-, ClO_3^- and ClO_4^-) detected by ion chromatography.

Transformation of fluoxetine by active chlorine was thus an additional degradation route, occurring

15

354   in concomitance with oxidation by oxygen radicals, presumably coagulation with $Fe(OH)_3$, and

355   UVA photolysis. The total amount of F^- ion at 60 min was 3.0 mg L^{-1}, which means that 46% of the

356   initial F atoms where still contained in fluorinated by-products. The N atom of fluoxetine, as shown

357   in Fig. S4, was very slowly converted into NO_3^- (only up to 0.12 mg L^{-1}). Neither NO_2^- nor NH_4^+

358   ions were detected and dissolved TN was constant. Hence, the solution at 60 min contained many

359   *N*-rich derivatives. From this analysis, the following reaction can be proposed for total

360   mineralization of fluoxetine:

361    $C_{17}H_{19}F_3NO^+ + 36\ H_2O \rightarrow 17\ CO_2 + 3\ F^- + NO_3^- + 91\ H^+ + 86\ e^-$ (8)

362   In order to assess the limits of PEF treatment with 0.1 mM Fe(III)–EDDS (1:1) complex to

363   degrade fluoxetine using the IrO_2/air-diffusion cell at 50 mA, the effect of the initial drug

364   concentration on the decay kinetics and the complex disappearance is presented in Fig. 2. Total

365   disappearance within 60 min was obtained for fluoxetine concentrations up to 0.147 mM (i.e., 30

366   mg L^{-1} TOC, Fig. 2a), whereas incomplete abatements resulted from more polluted solutions. This

367   means that the oxidation (and coagulation) ability of the system gradually approached its maximal,

368   as expected from the action of a quite constant amount of $^\bullet OH$, along with other oxygen radicals,

369   active chlorine and $Fe(OH)_3$, on a larger number of fluoxetine molecules. Furthermore, the increase

370   in drug concentration also entailed the accumulation of a greater amount of intermediates that

371   consumed oxidants (and $Fe(OH)_3$). The slower degradation kinetics was reflected in the decreasing

372   apparent rate constant, from $k_1 = 0.0986$ min^{-1} ($R^2 = 0.987$) at 0.049 mM fluoxetine to 0.0659 min^{-1}

373   ($R^2 = 0.998$) at 0.147 mM and 0.0226 min^{-1} ($R^2 = 0.997$) at 0.490 mM. On the other hand, Fig. 2b

374   informs about the slower degradation of the Fe(III)–EDDS complex as the initial fluoxetine content

375   became higher, which confirms the protective role of the organic pollutants mentioned above. In

376   fact, at the two highest fluoxetine concentrations, the complex was not completely destroyed at 60

377   min. Overall, these findings allow concluding that this PEF treatment was rather flexible, being

378   feasible: (i) to quickly destroy micropollutants at low concentrations and (ii) to completely remove

16

pollutants from more contaminated solutions, more slowly, thanks to the larger stability of the catalytic complex.

Trying to achieve a faster drug decay by the Fe(III)–EDDS-catalyzed PEF treatment, the effect of the applied current was investigated. As can be observed in Fig. 3, the value of 50 mA employed so far can be actually considered as the optimum one. The disappearance was much quicker than that at 10 mA ($k_1 = 0.0559$ min^{-1}, $R^2 = 0.998$), which additionally only attained a partial drug abatement, and slightly faster than that at 25 mA (0.0986 min^{-1} vs 0.0933 min^{-1}). At 75 mA, the profile was a bit better, but the incremental energy cost was not accompanied by a substantial enhancement of the decontamination rate. For this reason, no greater currents were tested. In any case, it is evident that the applied current did not have a preponderant influence on the process performance. This allows considering the UVA irradiation as the core of this modified PEF process, since the photoreduction of the complex via reaction (5) is the key step to provide Fe^{2+} needed for $^{\bullet}$OH production. Since photoreduction has its own limited kinetics, a current increase mainly causes an excessive accumulation of H$_2$O$_2$ (reaction (1)) that cannot find enough Fe^{2+} ions. Therefore, the excess of H$_2$O$_2$ was partly used in parasitic reactions that consumed $^{\bullet}$OH and IrO$_2$($^{\bullet}$OH), such as reaction (S4).

As a preliminary study to further expand the use of Fe(III)–EDDS-catalyzed PEF process to urban wastewater treatment, some trials were carried out in model matrices with other electrolytes (always maintaining the same conductivity), trying to reveal the effect of anions typically found in such wastewater. In Fig. S5, the degradation profile in 0.043 M Na$_2$SO$_4$ + 0.013 M NaCl medium was exactly the same as that already commented in 0.050 M Na$_2$SO$_4$. Note that such concentration of Cl$^-$ ion is typical in secondary effluents from WWTFs (see subsection 2.2). Hence, this similarity suggests that, although active chlorine could potentially contribute to fluoxetine degradation, Cl$^-$ ion is also a hydroxyl radical scavenger that reduces the oxidation power of the PEF system. Chlorine radicals resulting from reactions (S15)-(S19) are less powerful and more selective than

hydroxyl radical, which is detrimental for fluoxetine transformation. Similarly, CO_3^{2-} and HCO_3^- ions are known to scavenge the hydroxyl radicals via reactions (S22) and (S23) with fast kinetic constants. As a result, the decay of fluoxetine concentration in a 0.042 M Na_2SO_4 + 0.009 M $NaHCO_3$ mixture at natural pH ~ 8 was much slower, with only 77% disappearance at 60 min. In fact, such percentage was quite stable from ca. 30 min of electrolysis, which can be related to the presumed destruction of the catalytic complex around that time. Based on these results, it will be necessary to carry out some pre-treatment before addressing the PEF treatment of urban wastewater.

3.2. Fluoxetine degradation in urban wastewater

Fig. 4 highlights the normalized fluoxetine concentration decays during the PEF treatment of 0.049 mM drug solutions prepared in urban wastewater, using the IrO_2/air-diffusion cell at 50 mA. Considering the characteristics of the wastewater summarized in subsection 2.2, it is important to mention that the solutions with the spiked drug contained almost 20 mg L^{-1} TOC, which is twice the value of most of the solutions studied in subsection 3.1, and their natural pH was 7.2.

The PEF treatments of Fig. 4a were made with 0.1 mM Fe(III)–EDDS (1:1) complex at natural pH 7.2. Using the raw wastewater, the drug disappearance at 60 min was as low as 53% instead of 100% attained in 0.050 M Na_2SO_4 M (Fig. 1b). The higher TOC content may have a negative impact on the process performance, although probably of minor importance because Fig. 2a informed about the complete fluoxetine disappearance working up to 30 mg L^{-1} TOC. Therefore, the slower decay in wastewater can be rather accounted for by its particular composition, since it contained: natural organic matter (NOM) that competitively consumed UVA photons and reacts with oxygen radicals, and ions that act as radical scavengers, as shown from Fig. S5. The first feature was inherent from the matrix, but a proper conditioning could modify the second one. To this purpose, CO_2 was stripped from the urban wastewater following the procedure explained in subsection 2.2. In the absence of CO_3^{2-} and HCO_3^- ions, a faster and larger fluoxetine disappearance, reaching 78%, can be seen in Fig.4. The lower transparency of the wastewater and

its higher pH were two additional characteristics that affected negatively to fluoxetine removal, impeding that complete removal could be obtained, since they decreased the Fe^{2+} regeneration from reaction (5) and stimulated the precipitation of Fe(III) as $Fe(OH)_3$. Note that after 60 min of treatment in water without and with stripping, the initial pH decayed down to 6.2 and 4.6, respectively. Based on the positive influence of stripping, all subsequent trials were made with conditioned urban wastewater.

For the same PEF treatment, the effect of solution pH is shown in Fig. 4b. As expected, a better performance was obtained at more acidic pH, achieving 51%, 78%, 86% and 94% at pH 9.0, 7.2, 5.0 and 3.0. A lower pH value ensured that, as EDDS became destroyed, a larger amount of iron ions was dissolved rather than precipitated. This promoted a larger $^{\bullet}OH$ production from conventional Fenton's reaction (with uncomplexed Fe^{2+}) and Fenton-like reaction (with uncomplexed Fe^{3+}). At higher pH, coagulation with $Fe(OH)_3$ acquired more relevance for fluoxetine degradation.

The effect of the Fe(III)–EDDS dosage at pH 7.2, keeping the 1:1 ratio, can be seen in Fig. 4c. It is interesting to remark that almost complete fluoxetine abatement was achieved using 0.20 mM of the catalytic complex, exhibiting a much faster decay during the 60 min as compared to PEF with 0.10 mM of complex. The inset depicts the pseudo-first-order kinetics for both trials, yielding a greater $k_1 = 0.0246$ min^{-1} ($R^2 = 0.996$) at 0.20 mM. The upgraded abatement is in agreement with a higher amount of Fe^{2+} formed upon Fe(III)–EDDS photoreduction, which eventually fostered a much larger production of $^{\bullet}OH$ from Fenton's reaction. Nonetheless, despite the evident enhancement of drug disappearance upon increase of the Fe(III)–EDDS dosage, it was significantly slower than that in 0.050 M Na_2SO_4 with 0.10 mM of complex ($k_1 = 0.0986$ min^{-1} , Fig. 1b).

The influence of another key parameter like the Fe(III):EDDS ratio, at pH 7.2, is depicted in Fig. 4d. In general terms, the performance was better as the relative EDDS amount was increased, although the greatest difference really appeared when PEF without EDDS was compared to all other

454   trials with EDDS. PEF with uncomplexed Fe(III) in the form of $Fe(ClO_4)_3$ yielded a very poor drug

455   concentration decay (17% at 60 min), which was radically lower than that in Na_2SO_4 (83%, Fig.

456   1b). Such bad result can be related to a larger iron precipitation due to the higher pH, as well as to

457   complexation with non-photoactive NOM components. In contrast, the use of the 1:2 complex

458   yielded a final abatement of 88%, being slightly superior to that obtained with the 1:1 complex.

459   Although the former complex has been reported to be less photoactive (Wu et al., 2014) and EDDS

460   contributes to scavenge some of the oxygen radicals, in practice the larger amount of EDDS

461   contributed to iron solubilization for longer time, ending in a faster fluoxetine degradation.

462   The PEF treatment catalyzed with 0.20 mM Fe(III)–EDDS (1:1), which has been the most

463   successful in wastewater as discussed from Fig. 4c at 50 mA, was assessed in terms of the influence

464   of the applied current using the IrO_2/air-diffusion cell. As evidenced in Fig. S6a, the behavior was

465   globally similar to that found in Na_2SO_4. The lowest current (25 mA) was insufficient to yield the

466   complete disappearance of fluoxetine, since the NOM components consumed most of the H_2O_2

467   produced at the cathode. A higher current like 50 mA was optimal to electrogenerate enough H_2O_2

468   that was able to react with photogenerated Fe^{2+} and then create $^{\bullet}OH$. A further increase in applied

469   current was not efficient because the excess of H_2O_2 was wasted in parasitic reactions, as deduced

470   from the analogous profile at 75 mA. Fig. S6b shows that when the IrO_2-based anode was replaced

471   either by BDD or a RuO_2-based anode, at 50 mA, the decay profiles were exactly the same. This

472   confirms that the dominant contribution to fluoxetine disappearance came from $^{\bullet}OH$ generated in

473   the bulk via Fenton's reaction, rather than from $M(^{\bullet}OH)$ adsorbed on the anode surface.

474   To gain further insight into the effect of the $Fe(OH)_3$ precipitate on the performance of PEF

475   process, an additional study was performed with solutions containing 0.049 mM drug and 0.050 M

476   Na_2SO_4 at pH 7.2. Fig. S7 shows that, in the presence of 0.10 mM $Fe_2(SO_4)_3$, only 5.4% of

477   fluoxetine was abated at 60 min, suggesting a low coagulation ability of the $Fe(OH)_3$ precipitate

478   formed. This means that coagulation plays a minor role during the disappearance of fluoxetine.

479   Several electrochemical treatments were carried out using the IrO_2/air-diffusion cell, at 50 mA. Fig.

480   S7 evidences a higher drug decay (24%) in EO (i.e., without iron salt), which was upgraded in

481   homogeneous PEF (36%) and even more in heterogeneous PEF (60%). In the case of homogeneous

482   PEF, the solution containing fluoxetine, Na_2SO_4 and $Fe_2(SO_4)_3$ was previously filtered, yielding

483   0.13 mg L^{-1} of dissolved Fe^{3+}. These results corroborate the oxidation of fluoxetine by $IrO_2(^\bullet OH)$ at

484   the anode as well as by homogeneous $^\bullet OH$ formed from the photo-Fenton (2) and Fenton's reaction

485   (S1). Furthermore, the much greater drug decay found in heterogeneous PEF corroborates its

486   oxidation via heterogeneous Fenton's reaction occurring at the $Fe(OH)_3$ surface.

487   Although the main goal of this work was to investigate the ability of the Fe(III)–EDDS-

488   catalyzed PEF process to remove a target organic pollutant from urban wastewater, its

489   mineralization ability was also tested. In previous assays, it has been demonstrated that the catalytic

490   complex became gradually degraded, which means that the decontamination occurred in two

491   consecutive stages: (i) the first one, where the $^\bullet OH$ formed from Fenton's reaction had the leading

492   role, followed by (ii) a second one, where fluoxetine by-products and organic components from the

493   wastewater were destroyed by the adsorbed $M(^\bullet OH)$. During all the treatment, coagulation with

494    $Fe(OH)_3$ could also contribute to global mineralization, but with a minor role, as confirmed above.

495   Aiming to enhance the oxidation power of the system, a BDD/air-diffusion cell and a higher current

496   (100 mA) were employed to carry out these trials. Much lower TOC abatements were obtained

497   using the IrO_2 and RuO_2 anodes due to their lower ability to produce oxidizing agents able to

498   destroy the intermediates of fluoxetine and EDDS.

499   Fig. 5a shows the TOC decay trends for the PEF treatment of conditioned urban wastewater at

500   pH 7.2 under three different conditions: with 0.10 mM Fe(III)–EDDS, either without or with 0.049

501   mM fluoxetine, and with 0.20 mM of complex in the presence of fluoxetine. A similar decay rate

502   can be observed in all cases, achieving close TOC removal percentages around 50% at 300 min.

503   This means that a higher residual TOC was present in the final solution as the initial content was

21

504 increased. Hence, although the use of 0.20 mM Fe(III)–EDDS accelerated the decay of fluoxetine

505 concentration (Fig. 4c), the TOC content at the end of the electrolysis was higher (20.8 mg L^{-1}),

506 probably due to a slower removal of the products of EDDS. PEF process is known to yield great

507 TOC abatements, usually higher than 90%. The incomplete TOC removal found in this study can

508 then be mainly accounted for by the very poor contribution of photodecarboxylation by reaction (9).

509 Since most of the iron was precipitated during the first degradation stage, the refractory oxidation

510 by-products like carboxylic acids (Salazar et al., 2017) tended to become largely accumulated in the

511 solution. In conventional PEF at acidic pH, such molecules form complexes with Fe(III) that are

512 very photoactive, but in the Fe(III)–EDDS-catalyzed PEF their photodegradation only occurred

513 before EDDS destruction. Afterwards, all these intermediates were only degraded by BDD($^\bullet$OH),

514 probably with a minor contribution from coagulation with $Fe(OH)_3$.

515 $$Fe(OOCR)^{2+} + h\nu \rightarrow Fe^{2+} + CO_2 + R^\bullet \tag{9}$$

516 In spite of yielding only a partial TOC abatement, it was more relevant to investigate the ability

517 of the PEF process to reduce the overall toxicity. In Fig. 5b, the time course of toxicity (as EC_{50})

518 during the treatment of 0.049 mM fluoxetine in wastewater employing 0.10 mM Fe(III)–EDDS

519 (1:1) complex (Fig. 5a) is depicted. The toxicity increased during the first 60 min, which can be

520 explained by the generation of *N*- and *F*-rich toxic reaction by-products (see subsection 3.3),

521 thereby showing a gradual decay. Higher EC_{50} values can be seen from 60 min, attaining a plateau

522 from 180 min. The final EC_{50} value was close to that of the raw urban wastewater (80-90 mg L^{-1}).

523 This result suggests that, although only 50% of TOC removal could be achieved at 300 min,

524 detoxification was ensured. The absence of chlorine oxyanions (Fig. S4), the drug transformation

525 into innocuous compounds and the generation of non-toxic products from EDDS justifies this trend.

526 *3.3. Primary reaction by-products and mechanism for pollutant degradation*

527   The GC-MS analysis of the organic compounds extracted upon different treatments revealed

528   the generation of several by-products, which confirms the presence of nitrogenated and fluorinated

529   aromatic derivatives at short electrolysis time, as mentioned above.

530   Table 1 collects the intermediates detected after 20 min of Fe(III)–EDDS-catalyzed PEF

531   treatment of fluoxetine in 0.050 M Na_2SO_4 (i.e., trial of Fig. 1a). *N*-demethylation of fluoxetine (**1**)

532   yielded an aminoderivative (**2**). Alternatively, upon C–O bond cleavage, fluoxetine could be split

533   into two halves: 4-trifluoromethyl-phenol (**3**), which has been reported by Salazar et al. (2017) as

534   well, and the *N*-derivative 3-phenylpropenal (**5**). If the previous cleavage occurred upon

535   hydroxylation with $^{\bullet}OH$ and M($^{\bullet}OH$), a similar transformation was observed but with the

536   generation of a deaminated derivative (**4**). Some of the aromatic structures could be successively

537   converted to styrene (**6**), benzaldehyde (**7**) and benzoic acid (**8**), whereas those that kept the lateral

538   chain with the N atoms could experience internal cyclization to yield a quinolone (**9**). Finally, acetic

539   acid, in the form of an ester (**10**), was formed as one of the aliphatic short-chain carboxylic acids

540   that are persistent to oxidation, thus justifying the high final TOC commented above.

541   The by-products detected under analogous conditions but in the wastewater matrix (i.e., trial of

542   Fig. 4c, but using 0.20 mM Fe(III)–EDDS) are summarized in Table S3. Fluoxetine (**1**) was

543   converted to compound (**2**), but in this case the formation of the trifluorinated derivative (**3**) was

544   accompanied by the accumulation of a different aromatic molecule (**11**). The sequential route

545   yielding consecutive compounds (**6-8**), as well as the internal cyclization to yield the cyclic amine

546   (**9**) were confirmed. Nevertheless, the main characteristic in urban wastewater was the production

547   of two chloro-organic derivatives: compound **12** appeared upon chlorination of **3**, whereas

548   compound **13** could be formed from chlorination in $-CF_3$ position of **12**, followed by esterification

549   with phenylacetic acid. These chloro-aromatic molecules contributed to the enhanced toxicity

550   during the first 60 min (Fig. 5b). In addition, two organic components of wastewater namely **WW5**

and **WW7** (Table S2) still remained as part of the TOC determined. Fig. 6 presents the proposed

degradation route for fluoxetine.

Based on the trends highlighted above for fluoxetine, TOC and iron species, a very detailed

mechanism for the Fe(III)–EDDS-catalyzed PEF treatment in urban wastewater at near-neutral pH

is proposed in Fig. 7. To simplify, hydrated Fe^{2+} and Fe^{3+} have been written as Fe(II) and Fe(III).

The main characteristic of the Fe(III)–EDDS complex is its great photoactivity, yielding Fe(II)

either chelated with EDDS or in the uncomplexed form as written in reaction (5). The powerful

oxidant $^{\bullet}OH$ is then generated upon participation of electrogenerated H_2O_2. In addition, the catalytic

complex can react with H_2O_2 to produce $HO_2^{\bullet}$, or be gradually degraded by $^{\bullet}OH$ and $M(^{\bullet}OH)$. As a

minor route, it can be electroreduced to Fe(II)–EDDS. The products of all these reactions, namely

Fe(II), Fe(III) and Fe(II)–EDDS, then give rise to some crucial routes. At near-neutral pH and in the

presence of O_2, free and complexed Fe(II) tend to be oxidized to free Fe(III), which is photoreduced

via photo-Fenton reaction or precipitated as $Fe(OH)_3$ once the EDDS becomes degraded. As shown

in Fig. 7 and Table S1, several radicals can be formed. Considering all this, fluoxetine and NOM

components can be removed by: (i) direct anodic oxidation, (ii) indirect oxidation via adsorbed

$M(^{\bullet}OH)$ and $^{\bullet}OH$ (and other oxygen radicals) in the bulk, as well as by active chlorine and chlorine

radicals (see reactions in Table S1), (iii) coagulation with $Fe(OH)_2$ and $Fe(OH)_3$ (with a minor role)

and (iv) direct phototransformation. Note that some iron precipitates might be photoactive, but this

is not shown in the mechanism because the photoactivity of $Fe(OH)_3$ is expected to be insignificant

(Pehkonen et al., 1993).

4. Conclusions

The total removal of organic pollutants like fluoxetine in urban wastewater at near-neutral pH

is feasible by a novel PEF process with Fe(III)–EDDS as catalyst. In particular, the use of an

IrO_2/air-diffusion cell at 50 mA with 0.20 mM of catalytic complex caused the disappearance of

fluoxetine in 60 min. Fe(III)-EDDS showed a greater photoreduction ability than uncomplexed

Fe(III). This, along with the larger solubility of iron ions, ended in a higher concentration of Fe(II)

ions and hence, a greater $^\bullet$OH production from Fenton's reaction. TOC abatement occurred in two

consecutive stages. In the first one, $^\bullet$OH had the leading role, accompanied by other oxygen

radicals. In a second stage, once the EDDS was degraded and most of iron ions became

precipitated, fluoxetine by-products and organic components from the wastewater were destroyed

by the adsorbed $M(^\bullet OH)$. During all the treatment, coagulation with $Fe(OH)_3$ also contributed to

global TOC decay, whereas active chlorine, chlorine radicals and heterogeneous Fenton's reaction

had a minor importance. Stripping of wastewater with nitrogen had a positive effect, since it

removed scavengers like CO_3^{2-} and HCO_3^-. A low current was enough to reach the best

performance, since the $^\bullet$OH production was limited by the Fe(III)-EDDS photodegradation kinetics.

An excess of H_2O_2 electrogeneration at higher current was detrimental because it consumed

hydroxyl radicals. TOC abatement was incomplete (50% at 300 min) due to poor contribution of

photodecarboxylation of refractory aliphatic by-products like carboxylic acids, which only occurred

before total EDDS destruction. However, total detoxification was ensured. In conclusion, this new

PEF treatment was quite flexible since it allowed the treatment of low concentrations of pollutants,

in a quicker manner, or high concentrations, more slowly, thanks to the larger stability of the

catalytic complex. A thorough mechanism for the removal of the organic matter has been proposed.

Acknowledgements

References

Alcocer, S., Picos, A., Uribe, A.R., Pérez, T., Peralta-Hernández, J.M., 2018. Comparative study for degradation of industrial dyes by electrochemical advanced oxidation processes with BDD anode in a laboratory stirred tank reactor. Chemosphere 205, 682-689.

Aveiro, L.R., Da Silva, A.G.M., Candido, E.G., Antonin, V.S., Parreira, L.S., Papai, R., Gaubeur, I., Silva, F.L., Lanza, M.R.V., Camargo, P.H.C., Santos, M.C., 2018. Application and stability of cathodes with manganese dioxide nanoflowers supported on Vulcan by Fenton systems for the degradation of RB5 azo dye. Chemosphere 208, 131-138.

Bagnis, S., Fitzsimons, M.F., Snape, J., Tappin, A., Comber, S., 2018. Processes of distribution of pharmaceuticals in surface freshwaters: implications for risk assessment. Environ. Chem. Lett. 16, 1193-1216.

Brillas, E., Sirés, I., 2015. Electrochemical removal of pharmaceuticals from water streams: Reactivity elucidation by mass spectrometry. TrAC-Trend. Anal. Chem. 70, 112-121.

Brillas, E., Sirés, I., Oturan, M.A., 2009. Electro-Fenton process and related electrochemical technologies based on Fenton's reaction chemistry. Chem. Rev. 109, 6570-6631.

Clarizia, L., Russo, D., Di Somma, I., Marotta, R., Andreozzi, R., 2017. Homogeneous photo-Fenton processes at near neutral pH: A review. Appl. Catal. B: Environ. 209, 358-371.

Clematis, D., Cerisola, G., Panizza, M., 2017. Electrochemical oxidation of a synthetic dye using a BDD anode with a solid polymer electrolyte. Electrochem. Commun. 75, 21-24.

Coria, G., Pérez, T., Sirés, I., Brillas, E., Nava, J.L., 2018. Abatement of the antibiotic levofloxacin in a solar photoelectro-Fenton flow plant: Modeling the dissolved organic carbon concentration-time relationship. Chemosphere 198, 174-181.

Cuervo Lumbaque, E., Salmoria Araújo, D., Moreira Klein, T., Lopes Tiburtius, E.R., Argüello, J., Sirtori, C., 2019. Solar photo-Fenton-like process at neutral pH: Fe(III)-EDDS complex formation and optimization of experimental conditions for degradation of pharmaceuticals. Catal. Today 328, 259-266.

622 Desbiolles, F., Malleret, L., Tiliacos, C., Wong-Wah-Chung, P., Laffont-Schwob, I., 2018.

623 Occurrence and ecotoxicological assessment of pharmaceuticals: Is there a risk for the

624 Mediterranean aquatic environment? Sci. Total Environ. 639, 1334-1348.

625 El-Ghenymy, A., Rodríguez, R.M., Brillas, E., Oturan, N., Oturan, M.A., 2014. Electro-Fenton

626 degradation of the antibiotic sulfanilamide with Pt/carbon-felt and BDD/carbon-felt cells.

627 Kinetics, reaction intermediates, and toxicity assessment. Environ. Sci. Pollut. Res. 21(14)

628 8368-8378.

629 Flores, N., Sirés, I., Garrido, J.A., Centellas, F., Rodríguez, R.M., Cabot, P.L., Brillas, E., 2016.

630 Degradation of *trans*-ferulic acid in acidic aqueous medium by anodic oxidation, electro-

631 Fenton and photoelectro-Fenton. J. Hazard. Mater. 319, 3-12.

632 Galia, A., Lanzalaco, S., Sabatino, M.A., Dispenza, C., Scialdone, O., Sirés, I., 2016. Crosslinking

633 of poly(vinylpyrrolidone) activated by electrogenerated hydroxyl radicals: A first step

634 towards a simple and cheap synthetic route of nanogel vectors. Electrochem. Commun. 62,

635 64-68.

636 Guelfi, D.R.V., Brillas, E., Gozzi, F., Machulek Jr., A., de Oliveira, S.C., Sirés, I., 2019a. Influence

637 of electrolysis conditions on the treatment of herbicide bentazon using artificial UVA

638 radiation and sunlight. Identification of oxidation products. J. Environ. Manage. 231, 213-

639 221.

640 Guelfi, D.R.V., Ye, Z., Gozzi, F., de Oliveira, S.C., Machulek Jr., A., Brillas, E., Sirés, I., 2019b.

641 Ensuring the overall combustion of herbicide metribuzin by electrochemical advanced

642 oxidation processes. Study of operation variables, kinetics and degradation routes. Sep. Purif.

643 Technol. 211, 637-645.

644 Huang, W., Brigante, M., Wu, F., Hanna, K., Mailhot, G., 2012. Development of a new

645 homogenous photo-Fenton process using Fe(III)-EDDS complexes. J. Photochem. Photobiol.

646 A: Chem. 239, 17-23.

647 Huang, W., Brigante, M., Wu, F., Mousty, C., Hanna, K., Mailhot, G., 2013. Assessment of the

648 Fe(III)−EDDS complex in Fenton-like processes: From the radical formation to the

649 degradation of bisphenol A. Environ. Sci. Technol. 47, 1952-1959.

650 Jennifer Ebele, A., Abou-Elwafa Abdallah, M., Harrad, S., 2017. Pharmaceuticals and personal care

651 products (PPCPs) in the freshwater aquatic environment. Emerging Contam. 3, 1-16.

652 Komtchou, S., Dirany, A., Drogui, P., Bermond, A., 2015. Removal of carbamazepine from spiked

653 municipal wastewater using electro-Fenton process. Environ. Sci. Pollut. Res. 22, 11513-

654 11525.

655 Komtchou, S., Dirany, A., Drogui, P., Robert, D., Lafrance, P., 2017. Removal of atrazine and its

656 by-products from water using electrochemical advanced oxidation processes. Water Res. 125,

657 91-103.

658 Kümmerer, K., 2019. From a problem to a business opportunity-design of pharmaceuticals for

659 environmental biodegradability. Sustain. Chem. Pharm. 12, 100136.

660 Lanzalaco, S., Sirés, I., Sabatino, M.A., Dispenza, C., Scialdone, O., Galia, A., 2017. Synthesis of

661 polymer nanogels by electro-Fenton process: investigation of the effect of main operation

662 parameters. Electrochim. Acta 246, 812-822.

663 Lanzalaco, S., Sirés, I., Galia, A., Sabatino, M.A., Dispenza, C., Scialdone, O., 2018. Facile

664 crosslinking of poly(vinylpyrrolidone) by electro-oxidation with IrO_2-based anode under

665 potentiostatic conditions. J. Appl. Electrochem. 48, 1343-1352.

666 Li, J., Mailhot, G., Wu, F., Deng, N., 2010. Photochemical efficiency of Fe(III)-EDDS complex:

667 $^•$OH radical production and 17β-estradiol degradation. J. Photochem. Photobiol. A: Chem.

668 212, 1-7.

669 Martínez-Huitle, C.A., Rodrigo, M.A., Sirés, I., Scialdone, O., 2015. Single and coupled

670 electrochemical processes and reactors for the abatement of organic water pollutants: A

671 critical review. Chem. Rev. 115(24), 13362-13407.

672   Mezzelani, M., Gorbi, S., Regoli, F., 2018. Pharmaceuticals in the aquatic environments: Evidence

673   of emerged threat and future challenges for marine organisms. Marine Environ. Res. 140, 41-

674   60.

675   Oriol, R., Sirés, I., Brillas, E., De Andrade, A.R., 2019. A hybrid

676   photoelectrocatalytic/photoelectro-Fenton treatment of Indigo Carmine in acidic aqueous

677   solution using TiO_2 nanotube arrays as photoanode. J. Electroanal. Chem. 847, 113088.

678   Panizza, M., Cerisola, G., 2009. Direct and mediated anodic oxidation of organic pollutants. Chem.

679   Rev. 109(12), 6541-6569.

680   Papoutsakis, S., Brites-Nóbrega, F.F., Pulgarin, C., Malato, S., 2015. Benefits and limitations of

681   using Fe(III)-EDDS for the treatment of highly contaminated water at near-neutral pH. J.

682   Photochem. Photobiol. A: Chem. 303-304, 1-7.

683   Pehkonen, S.O., Siefert, R., Erel, Y., Webb, S., Hoffmann, M.R., 1993. Photoreduction of iron

684   oxyhydroxides in the presence of important atmospheric organic compounds. Environ. Sci.

685   Technol. 27, 2056-2062.

686   Pérez, T., Coria, G., Sirés, I., Nava, J.L., Uribe, A.R., 2018. Electrosynthesis of hydrogen peroxide

687   in a filter-press flow cell using graphite felt as air-diffusion cathode. J. Electroanal. Chem.

688   812, 54-58.

689   Ribeiro, J., De Andrade, A.R., 2004. Characterization of RuO_2-Ta_2O_5 coated titanium electrode -

690   Microstructure, morphology, and electrochemical investigation. J. Electrochem. Soc. 151,

691   D106-D112.

692   Ridruejo, C., Centellas, F., Cabot, P.L., Sirés, I., Brillas, E., 2018. Electrochemical Fenton-based

693   treatment of tetracaine in synthetic and urban wastewater using active and non-active anodes.

694   Water Res. 128, 71-81.

695   Roth, H., Gendel, Y., Buzatu, P., David, O., Wessling, M., 2016. Tubular carbon nanotube-based

696   gas diffusion electrode removes persistent organic pollutants by a cyclic adsorption – Electro-

697   Fenton process. J. Hazard. Mater. 307, 1-6.

698   Safarzadeh-Amiri, A., Bolton, J.R., Cater, S.R., 1997. Ferrioxalate-mediated photodegradation of

699   organic pollutants in contaminated water. Water Res. 31(4), 787-798.

700   Salazar, C., Ridruejo, C., Brillas, E., Yáñez, J., Mansilla, H.D., Sirés, I., 2017. Abatement of the

701   fluorinated antidepressant fluoxetine (Prozac) and its reaction by-products by electrochemical

702   advanced methods. Appl. Catal. B: Environ. 203, 189-198.

703   Scialdone, O., Randazzo, R., Galia, A., Filardo, G., 2009. Electrochemical oxidation of organics at

704   metal oxide electrode: the incineration of oxalic acid at IrO_2-Ta_2O_5 (DSA-O_2) anode.

705   Electrochim. Acta 54(4), 1210-1217.

706   Sirés, I., Garrido, J.A., Rodríguez, R.M., Brillas, E., Oturan, N., Oturan, M.A., 2007. Catalytic

707   behavior of the Fe^{3+}/Fe^{2+} system in the electro-Fenton degradation of the antimicrobial

708   chlorophene. Appl. Catal. B: Environ. 72, 382-394.

709   Soriano-Molina, P., García-Sánchez, J.L., Alfano, O.M., Conte, L.O., Malato, S., Sánchez-Pérez,

710   J.A., 2018. Mechanistic modeling of solar photo-Fenton process with Fe^{3+}-EDDS at neutral

711   pH. Appl. Catal. B: Environ. 233, 234-242.

712   Soriano-Molina, P., Plaza-Bolaños, P., Lorenzo, A., Agüera, A., García-Sánchez, J.L., Malato, S.,

713   Sánchez-Pérez, J.A., 2019. Assessment of solar raceway pond reactors for removal of

714   contaminants of emerging concern by photo-Fenton at circumneutral pH from very different

715   municipal wastewater effluents. Chem. Eng. J. 366, 141-149.

716   Steter, J., Brillas, E., Sirés, I., 2016. On the selection of the anode material for the electrochemical

717   removal of methylparaben from different aqueous media. Electrochim. Acta 222, 1464-1474.

718   UNESCO, Emerging Pollutants in Water Series, Vol. 1, Pharmaceuticals in the Aquatic

719   Environment of the Baltic Sea Region – A Status Report, 2017.

720   Vidal, J., Huilñir, C., Santander, R., Silva-Agredo, J., Torres-Palma, R.A., Salazar, R., 2018.

721   Effective removal of the antibiotic Nafcillin from water by combining the Photoelectro-

722   Fenton process and Anaerobic Biological Digestion. Sci. Total Environ. 624, 1095-1105.

723   Villanueva-Rodríguez, M., Bello-Mendoza, R., Hernández-Ramírez, A., Ruiz-Ruiz, E.J., 2019.

724   Degradation of anti-inflammatory drugs in municipal wastewater by heterogeneous

725   photocatalysis and electro-Fenton process. Environ. Int. 40, 2436-2445.

726   Wang, C., Niu, J., Yin, L., Huang, J., Hou, L.-A., 2018. Electrochemical degradation of fluoxetine

727   on nanotube array intercalated anode with enhanced electronic transport and hydroxyl radical

728   production. Chem. Eng. J. 346, 662-671.

729   Wang, A., Zhang, Y., Zhong, H., Chen, Y., Tian, X., Li, D., Li, J., 2018. Efficient mineralization of

730   antibiotic ciprofloxacin in acid aqueous medium by a novel photoelectro-Fenton process

731   using a microwave discharge electrodeless lamp irradiation. J. Hazard. Mater. 342, 364-374.

732   Welcher, F.J., 1975. Standard Methods of Chemical Analysis, sixth ed, vol. 2, R.E. Krieger

733   Publishing Co, Huntington, New York, Part B.

734   Wu, Y., Passananti, M., Brigante, M., Dong, W., Mailhot, G., 2014. Fe(III)–EDDS complex in

735   Fenton and photo-Fenton processes: from the radical formation to the degradation of a target

736   compound. Environ. Sci. Pollut. Res. 21, 12154-12162.

737   Xu, A., Wei, K., Zhang, Y., Han, W., Li, J., Sun, X., Shen, J., Wang, L., 2017. A facile-operation

738   tubular electro-Fenton system combined with oxygen evolution reaction for flutriafol

739   degradation: Modeling and Parameters optimizing. Electrochim. Acta 246, 1200-1209.

740   Yahya, M.S., Oturan, N., El Kacemi, K., El Karbane, M., Aravindakumar, C.T., Oturan, M.A.,

741   2014. Oxidative degradation study on antimicrobial agent ciprofloxacin by electro-Fenton

742   process: Kinetics and oxidation products. Chemosphere 117, 447-454.

743 Yang, W., Zhou, M., Oturan, N., Li, Y., Oturan, M.A., 2019. Electrocatalytic destruction of
744   pharmaceutical imatinib by electro-Fenton process with graphene-based cathode.
745   Electrochim. Acta 305, 285-294.

746 Ye, Z., Brillas, E., Centellas, F., Cabot, P.L., Sirés, I., 2019a. Electrochemical treatment of
747   butylated hydroxyanisole: Electrocoagulation versus advanced oxidation. Sep. Purif. Technol.
748   208, 19-26.

749 Ye, Z., Brillas, E., Centellas, F., Cabot, P.L., Sirés, I., 2019b. Electro-Fenton process at mild pH
750   using Fe(III)-EDDS as soluble catalyst and carbon felt as cathode. Appl. Catal. B: Environ.
751   257, 117907.

752 Ye, Z., Sirés, I., Zhang, H., Huang, Y.-H., 2019c. Mineralization of pentachlorophenol by
753   ferrioxalate-assisted solar photo-Fenton process at mild pH. Chemosphere 217, 475-482.

754 Yuan, Z., VanBriesen, J.M., 2006. The formation of intermediates in EDTA and NTA
755   biodegradation. Environ. Eng. Sci. 23, 533-544.

756 Zhang, M.-H., Dong, H., Zhao, L., Wang, D., Meng, D., 2019. A review on Fenton process for
757   organic wastewater treatment based on optimization perspective. Sci. Total Environ. 670,
758   110-121.

759 Zhang, Y., Klamerth, N., Ashagre Messele, S., Chelme-Ayala, P., Gamal El-Din, M., 2016.
760   Kinetics study on the degradation of a model naphthenic acid by ethylenediamine-*N,N'*-
761   disuccinic acid-modified Fenton process. J. Hazard. Mater. 318, 371-378.

762 Zhou, M., Oturan, M.A., Sirés, I. (Eds.), Electro-Fenton Process: New Trends and Scale-Up,
763   Springer Nature, Singapore, 2018.
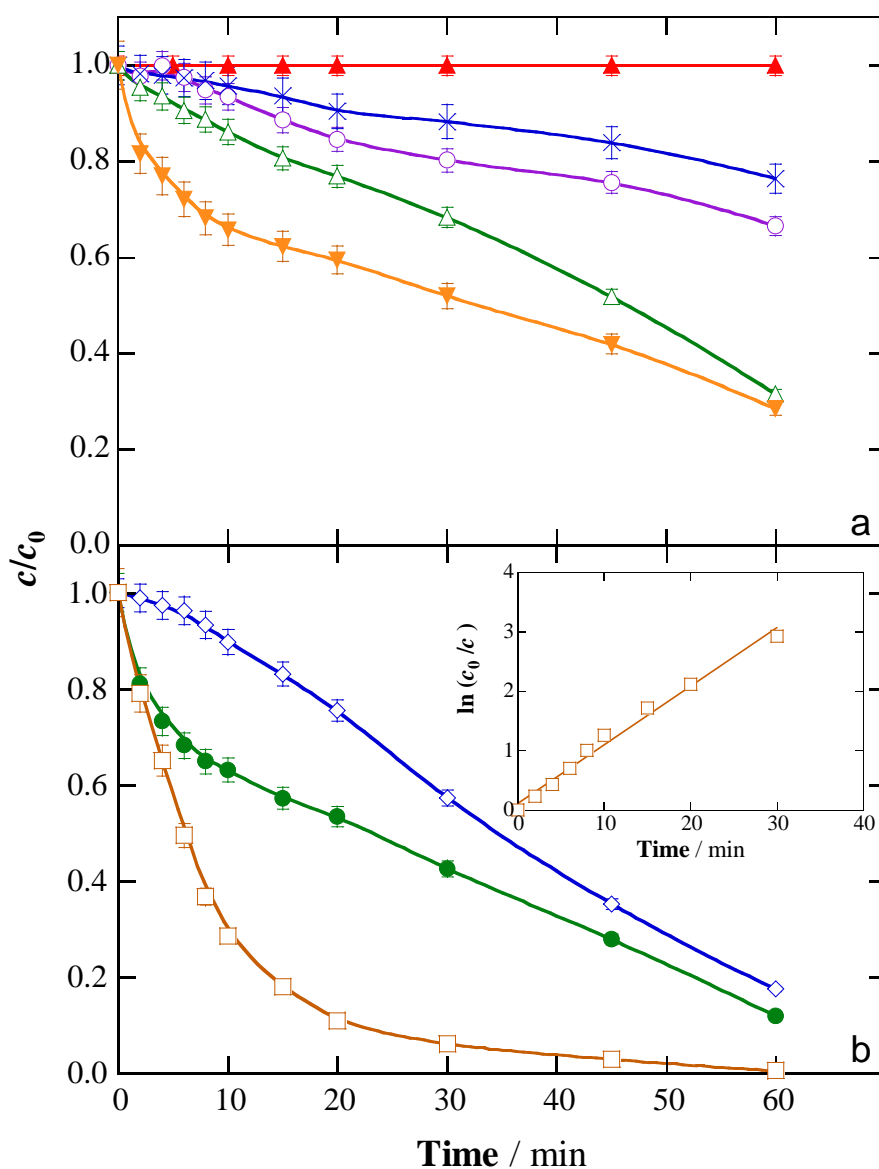
Fig. 1. Normalized fluoxetine concentration vs. electrolysis time during different treatments of 150 mL of 0.049 mM drug solutions with 0.050 M Na_2SO_4 at natural pH ~ 5.7. In the electrochemical assays, an IrO_2/air-diffusion cell was used at 50 mA and 25 °C. In (a), (▲) UVA photolysis, (◯) UVA photolysis with 0.10 mM Fe(III)–EDDS (1:1) complex, (×) EO, (△) EF with 0.10 mM Fe(III)–EDDS (1:1) complex and (▼) EF with 0.10 mM $FeSO_4$. In (b), (◇) PEF with 0.10 mM $Fe(ClO_4)_3$, (●) PEF with 0.10 mM $FeSO_4$ and (☐) PEF with 0.10 mM Fe(III)–EDDS (1:1) complex. The inset panel presents the pseudo-first-order kinetic analysis for the latter assay.
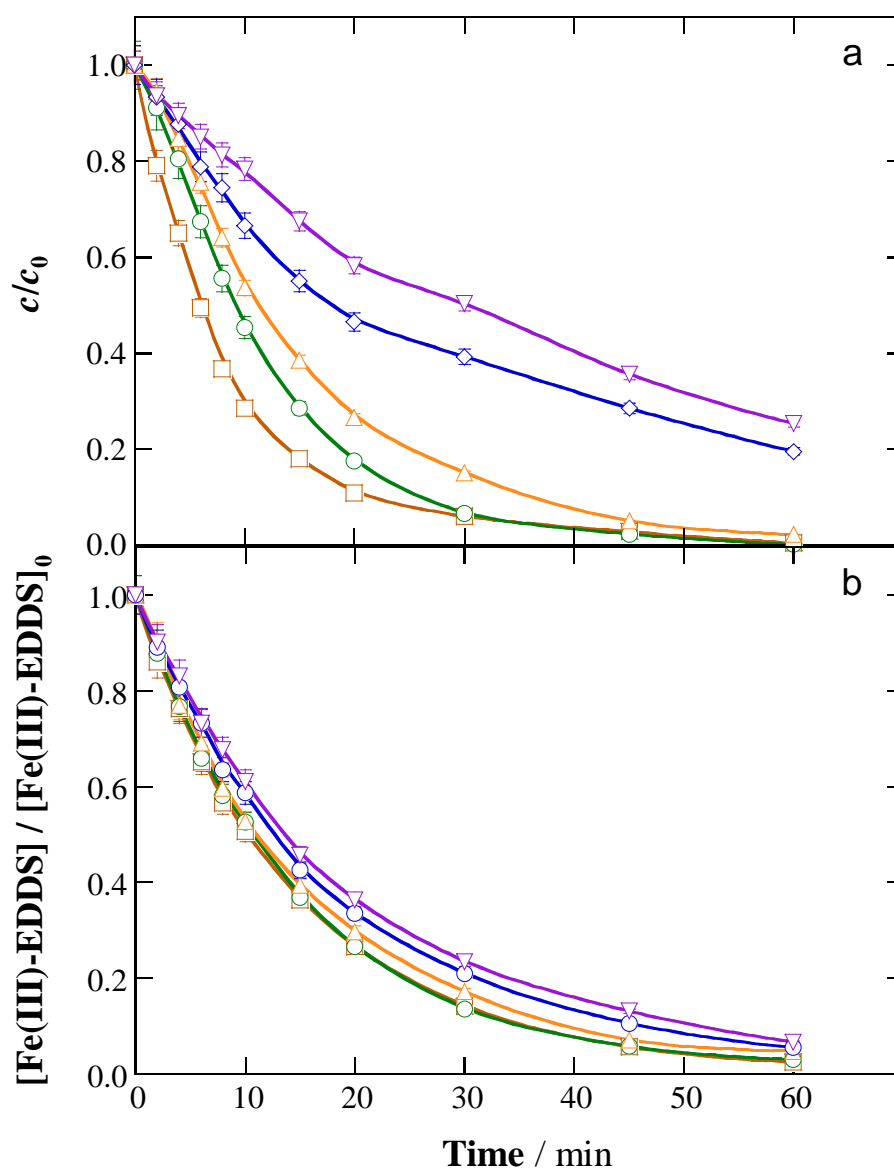
Fig. 2. Effect of fluoxetine concentration on the change of (a) normalized drug content and (b) normalized concentration of Fe(III)–EDDS (1:1) complex with electrolysis time during the PEF treatment of 150 mL of fluoxetine solutions with 0.10 mM Fe(III)–EDDS (1:1) complex and 0.050 M Na_2SO_4 at natural pH ~ 5.7 using an IrO_2/air-diffusion cell at 50 mA and 25 °C. Fluoxetine content: ($\square$) 0.049 mM, ($\bigcirc$) 0.098 mM, ($\triangle$) 0.147 mM, ($\diamondsuit$) 0.245 mM and ($\triangledown$) 0.490 mM.
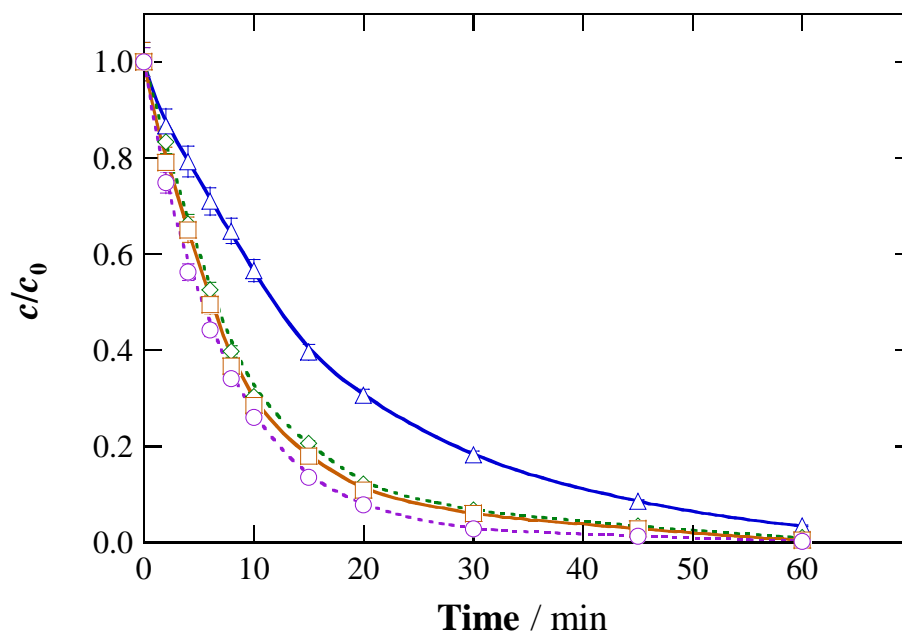
Fig. 3. Influence of applied current on the normalized fluoxetine concentration vs. electrolysis time during the PEF treatment of 150 mL of 0.049 mM drug solutions with 0.10 mM Fe(III)–EDDS (1:1) complex and 0.050 M Na_2SO_4 at natural pH ~ 5.7 and 25 °C using an IrO_2/air-diffusion cell. Current: ($\triangle$) 10 mA, ($\diamond$) 25 mA, ($\square$) 50 mA and ($\bigcirc$) 75 mA.
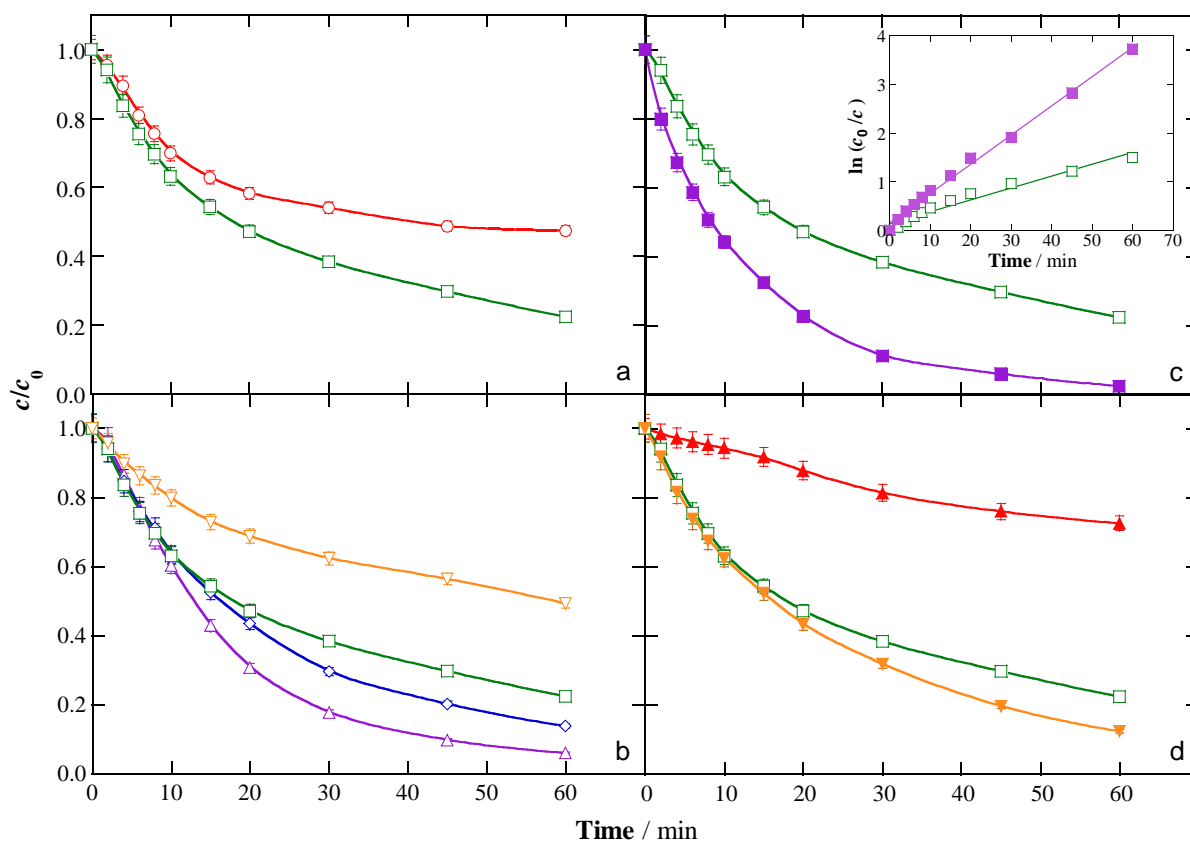
Fig. 4. Time course of normalized fluoxetine concentration during the PEF treatment of 150 mL of 0.049 mM drug solutions in urban wastewater using an IrO$_2$/air-diffusion cell at 50 mA and 25 °C. (a) (○) Without and (□) with stripping, employing 0.10 mM Fe(III)–EDDS (1:1) complex at natural pH 7.2. (b) With stripping, employing 0.10 mM Fe(III)–EDDS (1:1) complex at pH: (△) 3.0, (◇) 5.0, (□) 7.2 and (▽) 9.0. (c) With stripping, employing (□) 0.10 mM or (■) 0.20 mM Fe(III)–EDDS (1:1) complex at natural pH 7.2. The pseudo-first-order kinetic analysis is shown in the inset panel. (d) With stripping, employing (▲) 0.10 mM Fe(ClO$_4$)$_3$, (□) 0.10 mM Fe(III)–EDDS (1:1) complex and (▼) 0.10 mM Fe(III) + 0.20 mM EDDS complex, all at natural pH 7.2.
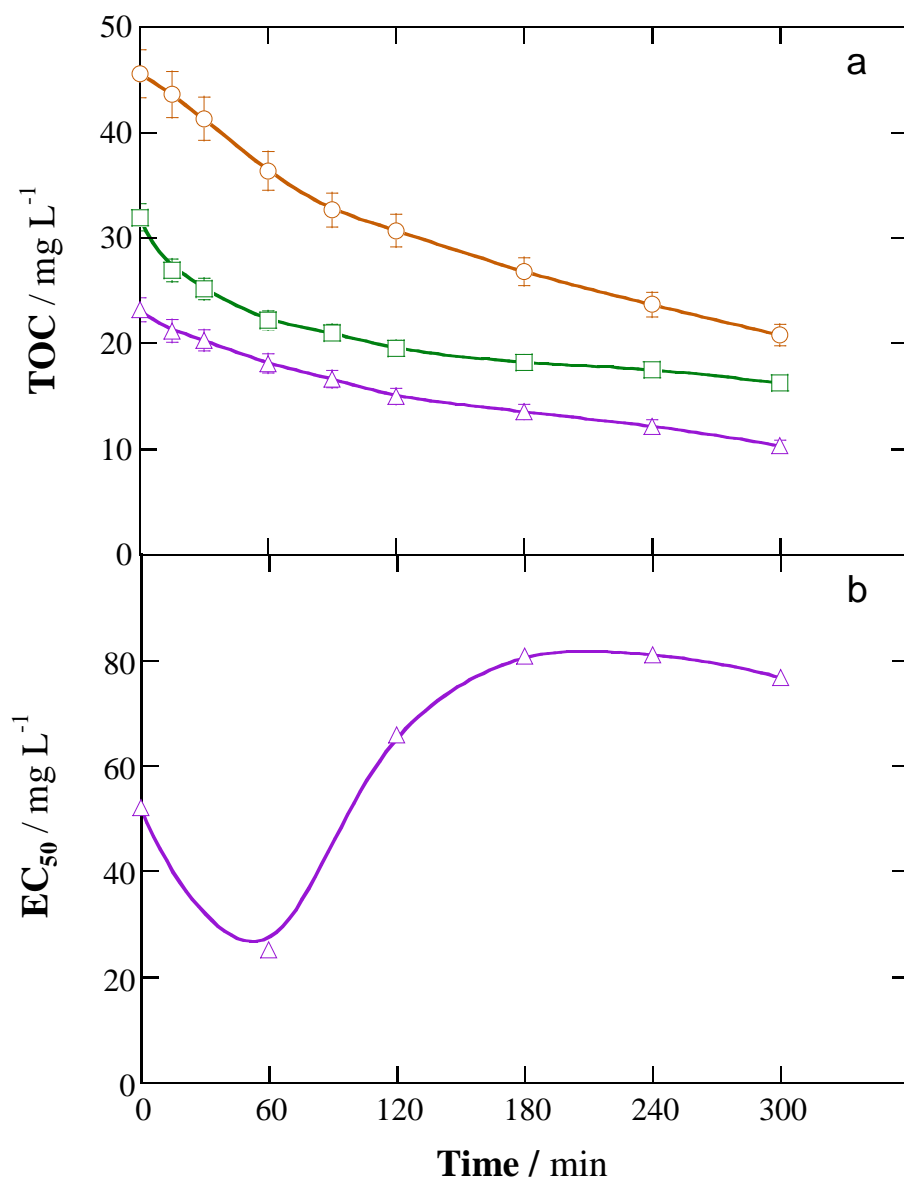
Fig. 5. (a) Change of TOC with electrolysis time during the PEF treatment of 150 mL of urban wastewater after stripping at natural pH 7.2 using a BDD/air-diffusion cell at 100 mA and 25 °C. The solution contained (△) 0.10 mM Fe(III)–EDDS (1:1) complex, without drug, (□) 0.049 mM fluoxetine + 0.10 mM Fe(III)–EDDS (1:1) complex and (○) 0.049 mM fluoxetine + 0.20 mM Fe(III)–EDDS (1:1) complex. (b) Time course of toxicity during the latter assay.
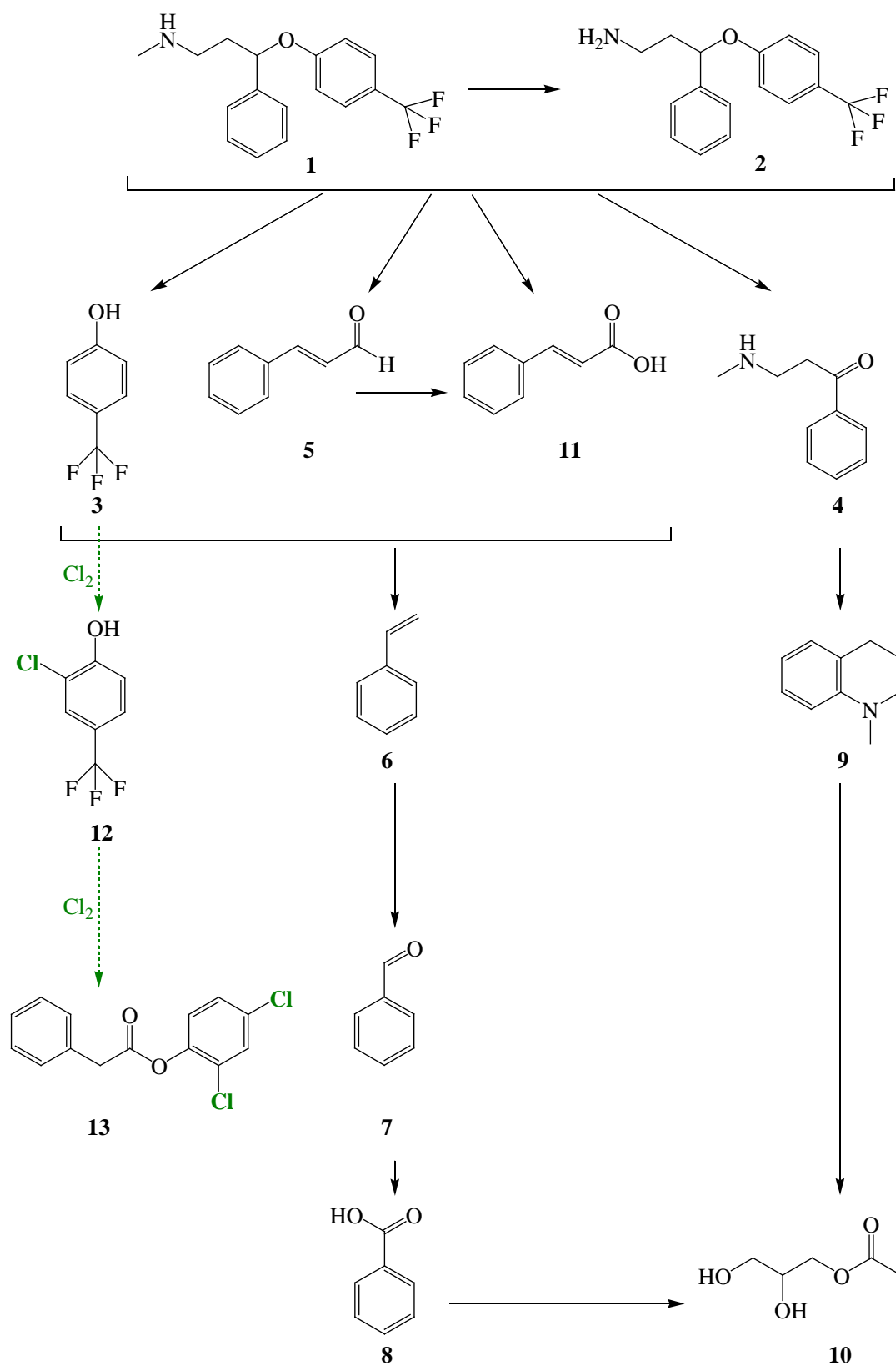
Fig. 6. Degradation route proposed for fluoxetine during the Fe(III)–EDDS-catalyzed PEF treatment at circumneutral pH. Chlorinated products detected in urban wastewater are highlighted in green.
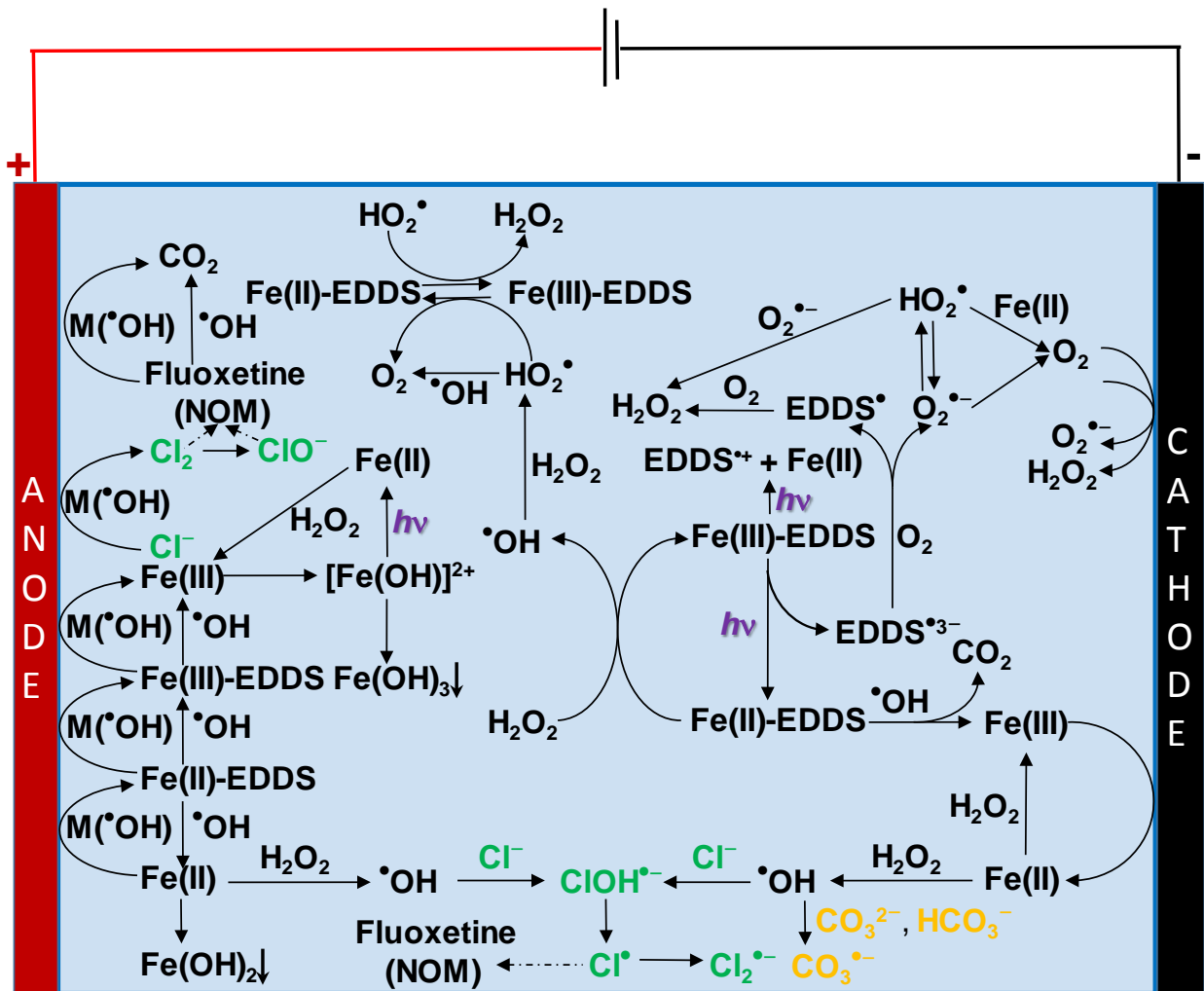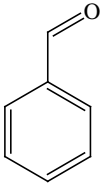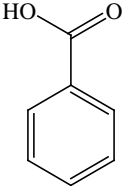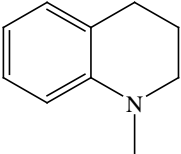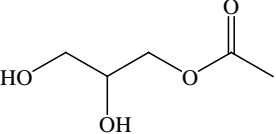
Fig. 7. Proposed mechanism for Fe(III)–EDDS-catalyzed PEF treatment at circumneutral pH.

Table 1.

Products detected by GC-MS using a non-polar (NP) or polar (P) column after 20 min of PEF treatment of 150 mL of a 0.049 mM fluoxetine solution with 0.10 mM Fe(III)–EDDS (1:1) complex and 0.050 M Na_2SO_4 at natural pH ~ 5.7 using an IrO_2/air-diffusion cell at 50 mA and 25 ℃.

Number	Chemical name	Molecular structure	Column	t_r (min)	Main fragments (m/z)
1	Fluoxetine		NP	34.11	309, 44
			P	39.60	
2	*N*-[3-Phenyl-3-(4-trifluoromethyl phenoxy)propyl] amine		NP	41.28	295, 190, 117, 86
3	4-Trifluoromethyl-phenol		NP	13.47	162, 143, 112
			P	32.54	
4	3-Methylamino-1-phenylpropan-1-one		NP	18.44	162, 149, 107, 78
5	3-Phenylpropenal		NP	16.63	131, 103, 77, 51
6	Styrene		P	11.94	104, 78, 51
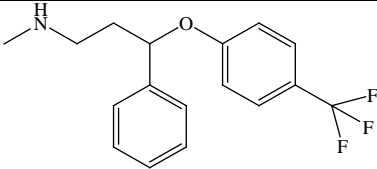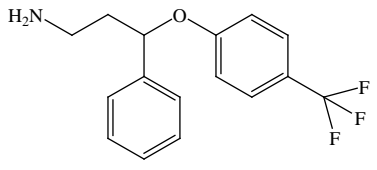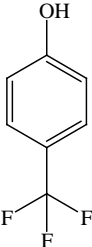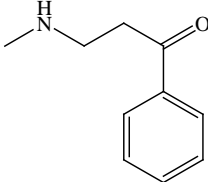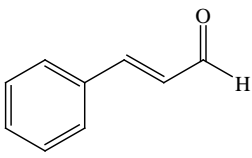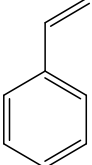
7	Benzaldehyde		NP	10.31	106, 77, 51
			P	18.7	
8	Benzoic acid		NP	20.52	122, 105, 77, 51
9	1-Methyl-1,2,3,4-tetrahydroquinoline		NP	21.16	147, 132, 118, 91
10	Acetic acid 2,3-dihydroxy propyl ester		NP	18.34	143, 103, 43